Geophysical Research Letters

Frequency-Dependent Moment Tensors of Induced Microearthquakes

Changpeng Yu[1,2] (iD), **Václav Vavryčuk[3]** (iD), **Petra Adamová[3]** (iD), and **Marco Bohnhoff[1,2]** (iD)

[1]Section 4.2 Geomechanics and Scientific Drilling, GFZ German Research Centre for Geosciences, Potsdam, Germany, [2]Institute of Geological Sciences, Free University of Berlin, Berlin, Germany, [3]Institute of Geophysics, The Czech Academy of Sciences, Prague, Czech Republic

Abstract Analysis of 984 induced microearthquakes from The Geysers geothermal reservoir in California reveals that the retrieved moment tensors depend on the frequency band of the inverted waveforms. The observed dependence is more significant for the percentages of the double-couple, compensated linear vector dipole, and isotropic (ISO) components than for the focal mechanisms. The average root-mean-square of the moment tensors obtained in different frequency bands is correlated with spectra of ambient noise. The percentages of double-couple and ISO components tend to decrease and increase with the upper cutoff frequency (f_u), respectively. This suggests that shear rupture radiates energy preferentially in a lower frequency band and tensile rupture in a higher frequency band. Events displaying a strong increase of the ISO with f_u are confined within the same depth interval as the injection points. This might be related to the strong thermoelastic effects in the vicinity of injection points that promote opening of small cracks adjacent to the main fractures.

Plain Language Summary Moment tensor (MT) describes shear and tensile motions in the earthquake source. The components of MT are usually assumed to be independent of the frequency. However, this assumption may not satisfy the complex rupture process of induced microearthquakes. We use a novel approach to investigate 984 induced microearthquakes from The Geysers geothermal reservoir in California and find that the retrieved MTs depend on the frequency band of input waveforms. The observed dependence is more significant for the components of MT measuring the proportions of seismic energy than for the components determining fault geometry. The component of MT describing shear motion shows a different frequency dependence than that describing tensile motion, suggesting that these two motions occur on the structures with different spatial scales. A subset of seismic events is identified to have a distinct feature of frequency dependence. These events only occur in the layer where the cool water is injected into the hot reservoir and do not migrate downward as the other events. This might be related to the strong thermal effects in the vicinity of injection points that promote the opening of small cracks adjacent to the main fractures.

1. Introduction

Source processes of induced microearthquakes are complex due to the presence of fluids and a mixture of shear and tensile rupturing (e.g., Martínez-Garzón et al., 2017; Šílený et al., 2009; Vavryčuk, 2002; Zhao et al., 2014). Rupture processes occur on various scales and radiate seismic energy in different frequency bands. For example, tensile opening of small wing cracks generate more high-frequency components than shear rupture along the main fracture (e.g., L. R. Johnson, 2014a; Vavryčuk, 2011a). However, this complexity is commonly ignored. Focal mechanisms are assumed to be frequency independent, and the seismic moment tensors (MTs) are typically calculated for a common source time function (Udías et al., 2014). As a consequence, different MTs can be reported for the same earthquakes if individual types of waves or full waveforms are inverted in different frequency bands, or if seismic data are recorded by instruments with different frequency responses.

In order to describe the source process more properly and in more detail, the MTs should be considered as frequency dependent and the broadband waveforms should be inverted for six independent MT rate functions (Ohminato et al., 1998; Ruff & Tichelaar, 1990; Šílený, 1998; Vavryčuk, 2011a) with no constraint to a common source time function. Such an approach is, however, data demanding and sensitive to details in the velocity model as well as computationally expensive. In particular, knowledge of the

frequency-dependent attenuation is critical and complicated to handle correctly in full waveform modeling because it might be different for different types of waves (Kinoshita, 1994; Yoshimoto et al., 1993). A simplified alternative approach is to invert individual wave types for MTs in a standard way (with a common source time function) but repeatedly in a number of different frequency bands. In this way, we get a set of MTs characterizing a rupture process of an earthquake at individual frequencies. This approach can efficiently be applied to a large number of microearthquakes to estimate the spatiotemporal variation and statistical properties of the source process.

The Geysers geothermal field in Northern California is the largest geothermal power facility in the world and has been in operation for more than 50 years. In recent decades, a large volume of fluid was injected into the reservoir to maintain the pressure and steam production. Consequently, the local seismicity rate was significantly enhanced (Beall et al., 2010; Dellinger et al., 2017; Majer & Peterson, 2007). Focal mechanisms and MTs of different subsets of events in this area were calculated using different waveform data and inversion schemes (Boyd et al., 2015, 2018; Guilhem et al., 2014; L. R. Johnson, 2014b; Kwiatek et al., 2015; Martínez-Garzón et al., 2014, 2017). In Yu et al. (2018), the field-wide variations of faulting regime, stress tensor, and ISO component were investigated using the full MTs of 1,421 induced microearthquakes recorded by a broadband seismic network. In this paper, we extend the analysis and use these broadband waveform recordings to investigate the frequency dependence of focal mechanisms and MTs for 984 induced microearthquakes from The Geysers area. The frequency dependence of the directions of the P/T axes and of the double-couple (DC), compensated linear vector dipole (CLVD), and isotropic (ISO) components is analyzed. The statistical properties of frequency-dependent MTs are extracted and interpreted. A particular focus is put on the frequency dependence of the ISO components to assess the impact of fluid injection on the source processes.

2. Data and Method

In the study of Yu et al. (2018), MTs of 1,421 microearthquakes with magnitudes ML $\geq$ 2.0 occurring throughout The Geysers field between June 2012 and June 2013 were studied. The field-wide dense network of 26 local broadband stations provided good azimuthal coverage as well as a broad frequency band of waveforms (see Figure S1 in the supporting information). The P wave amplitudes extracted from the broadband waveform data using the principal component analysis (PCA) method were inverted for MTs (Vavryčuk et al., 2017). The PCA-based MT inversion successfully suppresses the influence of station-dependent effects such as local noise and site effects, or source directivity. In comparison with the waveform inversion, it is less sensitive to inaccuracies in the velocity model and noise in the data. Moreover, this approach proves to be computationally very efficient (Vavryčuk et al., 2017).

Benefiting from the broadband data set and a high computational efficiency of the PCA-based MT inversion, 104 candidate MTs are calculated using eight band-pass filters and 13 time windows for each event. One lower cutoff frequency (f_l = 0.15 Hz) and eight upper cutoff frequencies (f_u = 2, 2.5, 3, 4, 5, 6, 7, and 8 Hz) are used to define the band-pass filters applied to the broadband waveforms. The 13 time windows ensure the P wave is correctly isolated for each filter. The P wave amplitudes are then extracted by the PCA method for MT inversion. The frequency dependence of MTs is mainly controlled by the upper cutoff frequency f_u, which will be an important parameter discussed in the following sections. The candidate MTs of one event are divided into eight groups according to f_u (Figure 1). Each group contains 13 MT solutions calculated using the same lower cutoff frequency f_l and 13 time windows.

All MTs are decomposed into the DC, CLVD, and ISO components (Knopoff & Randall, 1970; Vavryčuk, 2015) and evaluated by the root-mean-square (RMS) differences between the synthetic and observed amplitudes. The DC component describes the fault motion of shear rupture, and the ISO component describes the volumetric change of tensile rupture (Vavryčuk, 2011b, 2015). The CLVD component is correlated with the ISO component for tensile rupture. If the CLVD is observed together with zero ISO, it might indicate an irregular fracture geometry. This is, however, not a frequent case for induced microearthquakes, which are characterized by small ruptures. The CLVD might also be apparent, because it is more sensitive to errors in the inversion than the ISO component (Stierle, Bohnhoff, et al., 2014; Stierle, Vavryčuk, et al., 2014). The relative percentages of the DC, CLVD, and ISO components are calculated according to Vavryčuk, 2001, 2005) and represent the proportions of seismic energy radiated by these three force equivalents.
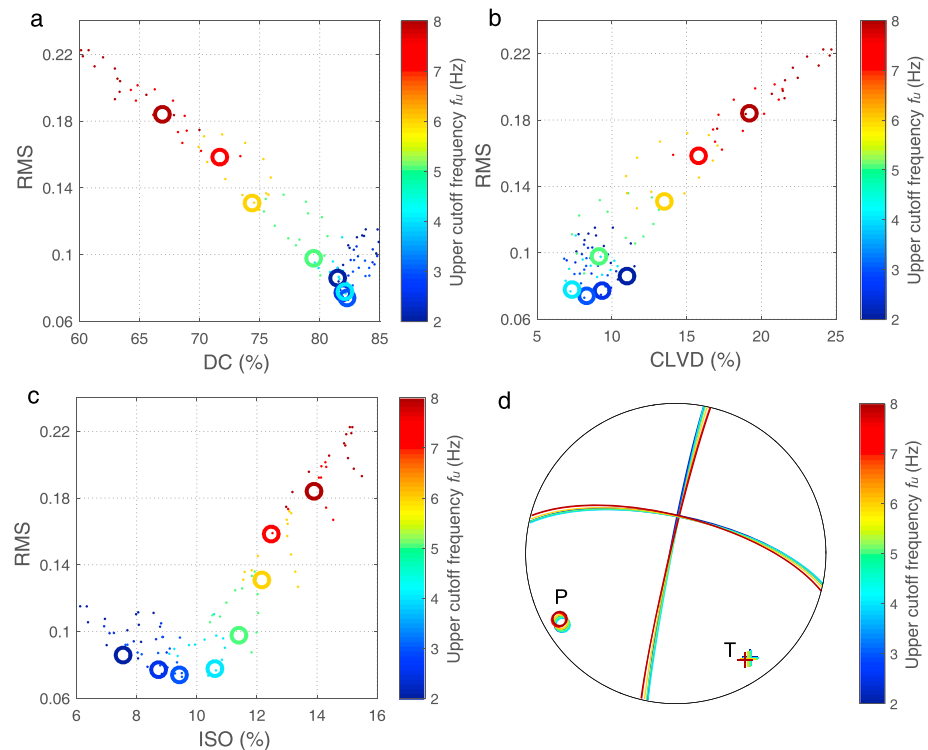
Figure 1. The percentages of (a) double-couple (DC), (b) compensated linear vector dipole (CLVD), and (c) isotropic (ISO) components, and the root-mean-square (RMS) of moment tensors (MTs; dots) calculated using different band-pass filters and time windows for one event. MTs are divided into eight groups according to the upper cutoff frequencies (color-coded). One optimal MT (circles) is determined for each group by averaging three MTs with the lowest RMS. (d) The fault plane solutions of eight optimal MTs.

A single optimal solution can be extracted from each group of MTs (defined by the same f_u) according to the RMS levels. As the candidate MTs in each group are not regularly sampled in the RMS-DC-CLVD-ISO space, the optimal solution is determined by averaging three MTs with the lowest RMS in each group. In this way, we get the most stable and reliable solutions. Then, eight optimal MTs corresponding to f_u are found for each event (Figure 1). By decomposing the optimal MTs, the frequency dependence of the DC, CLVD, and ISO components and the RMS as well as the P/T axes are evaluated for individual events.

Because of the complexity of source mechanisms, the frequency dependence of MTs for individual events varies and is not always as significant as shown in Figure 1. In order to present statistically significant results, we therefore analyze the frequency dependence of MTs for a subset of 984 events selected from 1,421 earthquakes according to the error limits estimated by adding random noise and perturbing the velocity model and event locations (see Yu et al., 2018). We determine the probability distributions of the DC, CLVD, ISO and RMS for each upper cutoff frequency f_u and calculate the corresponding mean values.

3. Results

3.1. Significance and Uncertainty of Frequency Dependence

As seen from Figures 1a to 1c, the optimal solutions of DC, CLVD, and ISO percentages extracted from each group according to the RMS levels display visible variations with f_u. By contrast, Figure 1d indicates that no significant changes of the fault plane solutions of the optimal MTs are observed for different frequency bands. In order to get robust results, ranges of five parameters; the DC, CLVD, and ISO percentages; and the orientations of P/T axes are calculated for a set of eight optimal MTs of each event (see Figure S2 in the supporting information). Then, the ranges are averaged over all analyzed events. According to the statistical distributions (see Figures 5 and 10 in Yu et al., 2018), the total variations of the DC, CLVD, and ISO percentages and of the orientations of the P/T axes are determined at the 95% confidence levels. The

Table 1
Significance of the Frequency Dependence of the DC, CLVD, and ISO Percentages and the P/T Axes

	Average range value[a]	Variation at 95% confidence level[b]			Significance[c]
		Start	End	Length	
DC (%)	14.51	35.40	94.24	58.84	0.25
CLVD (%)	15.56	-26.65	52.54	79.19	0.20
ISO (%)	4.60	-5.45	22.36	27.81	0.17
P axis (°)	6.45	0	86.64	86.64	0.07
T axis (°)	5.48	0	67.40	67.40	0.08

[a]The range values of different parameters averaged over all analyzed events. [b]The variations of different parameters at the 95% confidence level (Yu et al., 2018). [c]The ratio of the average range value and the width of confidence interval.

significance of the frequency dependence of each parameter is evaluated as the ratio of the average range and the width of the confidence interval (Table 1). The DC, CLVD, and ISO percentages have comparable levels of significance of the frequency dependence, which are much higher than that of the *P/T* axes. This means that increasing f_u appreciably affects the magnitude of different source components in the signal, but it has a minor influence on the fault plane geometry. This explains the reason of assuming a frequency-independent focal mechanism in previous studies, because the priority of most studies is to determine the fault plane solutions.

In addition to the physical process in the earthquake source, nonphysical factors such as ambient noise or unmodeled structure inhomogeneities may also affect the frequency dependence of MTs. As regard the ambient noise, the spectral analysis indicates that its level is highest at low frequencies. Then it decreases and reaches a minimum between 2 and 3 Hz, and it rises again at higher frequencies (Figure 2a). This causes a variation of the signal-to-noise (S/N) ratio with frequency (Figures 2b and S3 in the supporting information). Within the range of f_u (2–8 Hz), most of the studied events show a high S/N ratio from ~10^2 to ~10^4. According to the synthetic tests of the PCA-based MT inversion (Figure 5 in Vavryčuk et al., 2017), such levels of noise (~1–0.01%) can only result in variations of DC, ISO, and CLVD components less than 0.1%, which are negligible with respect to the observations in this study.

Since a 1-D velocity model is used in this study, we ignore scattered waves generated by small-scale velocity heterogeneities, which might become more prominent as the frequency increases. This could also bias the result of MTs in different frequency bands. Since the scattered waves are usually station-dependent, they can be viewed as "structure-generated" noise. Such type of noise is, however, very effectively suppressed by the PCA-based MT inversion (see Vavryčuk et al., 2017). Based on synthetic tests, noise generated by unknown details of the structure with a level up to 40% produces a bias in the ISO less than 0.25%. No tendency to producing preferentially positive values of the ISO was observed for noise levels up to 100%.

Although these nonphysical factors can change the RMS misfit of the MT inversion, their effects can be prevented by the PCA-based approach from being passed to the retrieved MTs. Figure 3 shows the probability distributions of the DC, CLVD, ISO, and RMS of the 984 analyzed events together with their mean values for each frequency f_u. The variation of the RMS with frequency shows a clear correlation with the spectra of ambient noise and the S/N ratio (Figures 3d and 3h). This suggests that ambient noise affects the RMS misfit of the MT inversion. However, the variations of the DC, CLVD, and ISO do not follow the tendencies of the RMS, noise, and the S/N ratio. The increasing uncertainty of MTs with the noise level is only reflected by more scattered distributions of the DC, CLVD, and ISO, resulting in widening of their probability density
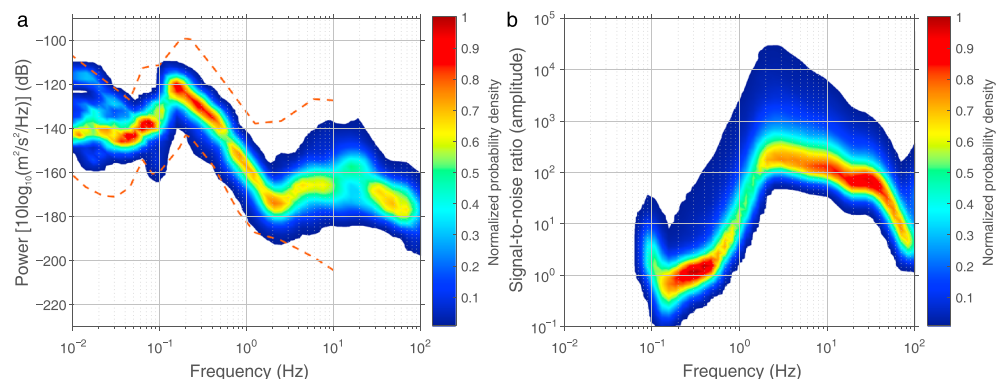

Figure 2. (a) Spectrum of the ambient noise recorded by the network of broadband stations in this study. The red curves are the global high and low noise models (Peterson, 1993). (b) Signal-to-noise ratio for all the studied events by comparing the spectra of noise and event signal.
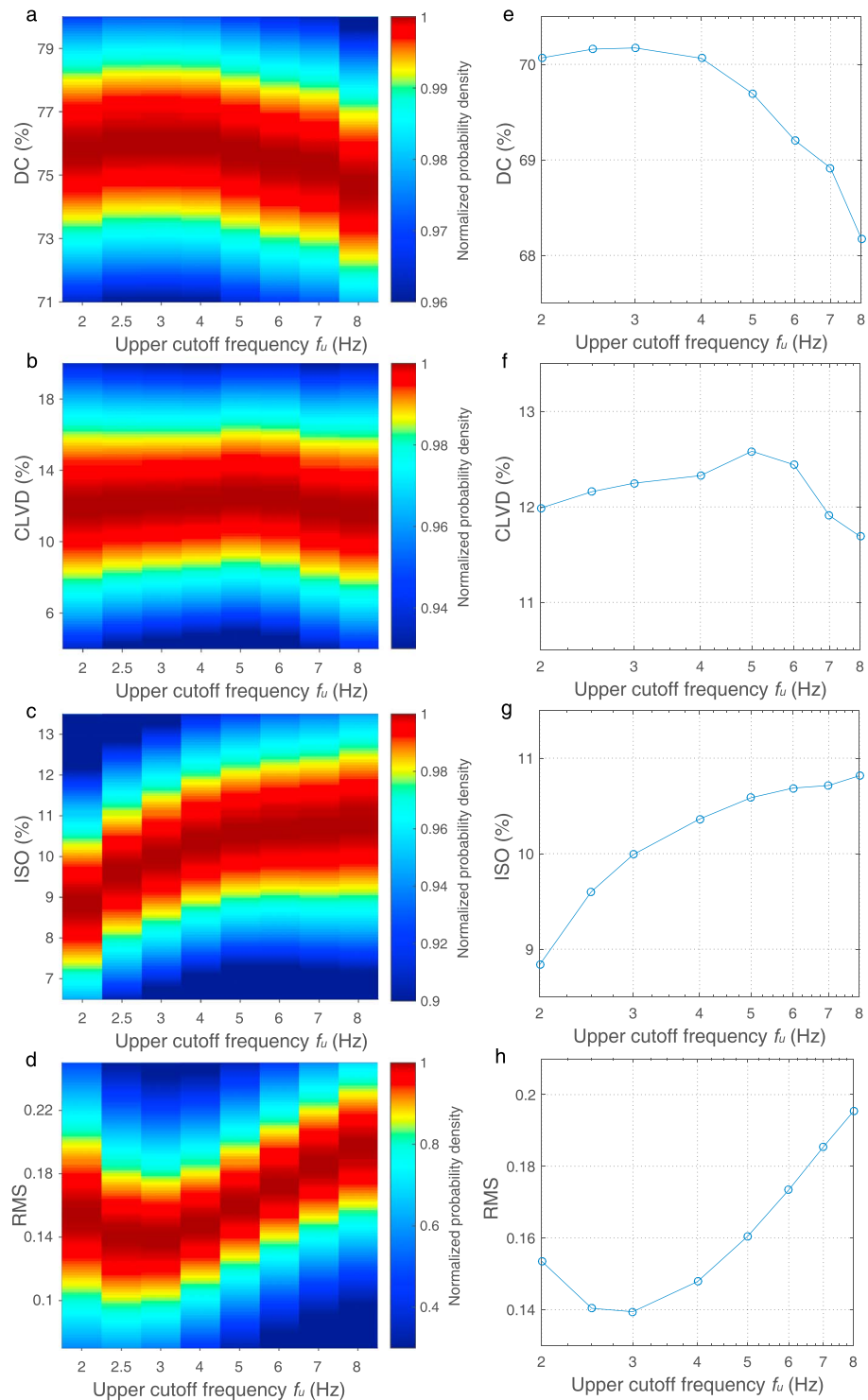
Figure 3. Probability distributions and the mean values of (a and e) DC, (b and f) CLVD, and (c and g) ISO percentages and (d and h) RMS values for all the 984 events along with eight upper cutoff frequencies.

functions at the frequencies with a higher RMS (see Figures 3a–3c). The tendencies of the mean values of the probability distributions with f_u are stable and can reliably depict the frequency dependence of MTs related to the source process (Figures 3e–3g).

3.2. Statistical Properties of Frequency Dependence

As f_u increases, the frequency band is widened and more high-frequency portions are used in the MT inversion. The DC, CLVD, and ISO components show different statistical trends with f_u (Figure 3). The most notable features are the variations of the DC and ISO components, because they describe the properties of shear and tensile ruptures, respectively, that are two major mechanisms of induced microearthquakes. The percentage of the DC component decreases monotonically with increasing f_u (Figure 3e). Such trend suggests that seismic energy radiated by shear rupture is more prominent in lower frequency bands. By contrast, the percentage of the ISO component increases with increasing f_u (Figure 3g). This suggests that the tensile rupture tends to dominate at higher frequencies. The CLVD variation with f_u is not as significant as that of the DC and ISO. It shows irregular tendency being probably affected by errors of the inversion, in particular, for $f_u > 5$ Hz (Figure 3f). However, the notable variations of the DC and ISO with f_u support an idea that they are related to the physical conditions in the source.

The difference in frequency dependence of DC and ISO implies that shear and tensile ruptures radiate seismic energy preferentially in low- and high-frequency bands, respectively. This is also evidenced by spectra of shear and tensile components of moment rate functions for earthquakes in the West Bohemia swarm (Vavryčuk, 2011a). Similarly, L. R. Johnson (2014b) observed higher corner frequencies of the isotropic part than the deviatoric part of dynamic MTs for 20 microearthquakes in The Geysers area, though using both P and S waves in the waveform inversion complicates their interpretation because shear rupture itself can also result in different corner frequencies of the P and S waves (Madariaga, 1976; Sato & Hirasawa, 1973). According to these observations, it is conceivable that these two rupture processes occur at different spatial scales. For individual induced microearthquakes, shear rupture occurs along larger fractures or fault segments, while tensile rupture may preferentially occur on smaller cracks adjacent to the main fracture, such as wing cracks as proposed in Vavryčuk (2011a) and L. R. Johnson (2014a).

3.3. Frequency Dependence of the ISO Component

The ISO component describes a volumetric change of earthquake sources caused by tensile rupture. The spatiotemporal variation of the ISO component can directly be related to the injection and migration of fluids (Martínez-Garzón et al., 2017; Yu et al., 2018). Therefore, we performed a further analysis of the frequency dependence of the ISO component in order to investigate the effects of fluid injection and migration in the geothermal reservoir in more details.

For the whole set of events, the average percentage of the ISO component increases almost in a monotonic trend with increasing f_u. However, this does not mean that the ISO of individual events always displays the same tendency. In order to separate the events with a different frequency dependence, a linear fit of the ISO is performed in the whole range of frequency f_u (Figure 4a). The positive/negative correlation coefficients R and the slopes β quantify a degree of linearity of ISO with f_u and how strongly the ISO increases or decreases with f_u. The numbers of events with different correlation coefficients and slopes are shown in histograms (Figures 4b and 4c). For the events with a weak frequency dependence indicated by small absolute values of correlation coefficients and slopes ($|R| \leq 0.6$ and $|\beta| \leq 0.5$), the numbers of events with increasing or decreasing ISO components are comparable. However, for the events with a strong frequency dependence ($|R| \geq 0.6$ and $|\beta| \geq 0.5$), the contrast between these two groups is more pronounced (Figures 4b and 4c). Most of the events with a strong frequency dependence are characterized by the ISO increasing with f_u. This property probably reflects a common physical process occurring in the source.

The depth distributions of events with the increasing/decreasing ISO (Figure 4d, left panel, blue and orange) significantly differ at a depth interval of ~1-2 km with the largest difference at ~1.5 km, characterized also by the highest number of injection points (Figure 4d, right panel). It appears that the difference between these two groups of events is correlated with the injection points in the depth direction. To further illustrate such a correlation, a subset of events with extremely large correlation coefficients and slopes ($R \geq 0.8$ and $\beta \geq 1.0$) is extracted to represent the events with an extra significant increase of ISO with f_u. The depth distribution of these events (Figure 4d, left panel, green) is highly consistent with that of the injection points. These events are mostly confined within the main injection interval (~1-2 km) and do not migrate downward like the other events, which form a secondary maximum below the main injection interval. Such a particular
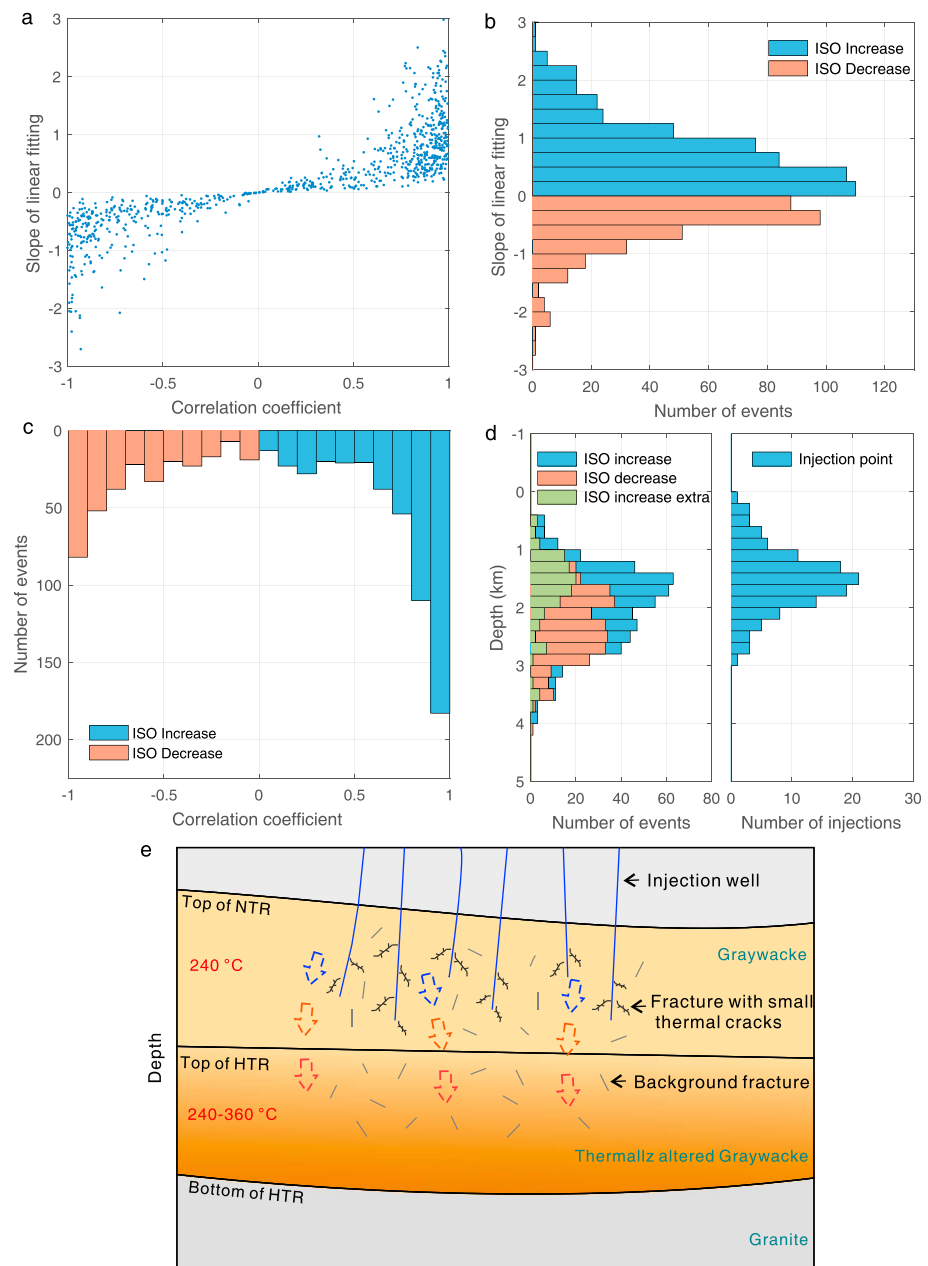
Figure 4. (a) The correlation coefficients and the slopes of the linear dependence between the percentage of the ISO component and the upper cutoff frequency. (b) The histograms of the slopes, and (c) the histograms the correlation coefficients. (d) The depth distributions of (left) the events with the increase and decrease of ISO component, and (right) the injection points. The events with large correlation coefficients (>0.8) and slopes (>1.0) are plotted in green. (e) Schematic diagram illustrating the distribution and the mechanism of events with an extra significant increase of ISO with f_u.

distribution suggests that these events are closely related to the fluid injection in the vicinity of injection points rather than to the fluid migration to the deeper reservoir.

The Geysers geothermal reservoir consists of the "normal" temperature reservoir (NTR) of ~240 °C and the underlying high-temperature reservoir (HTR) of ~240-360 °C (Beall & Wright, 2010; Stark, 2003). The cool water (~66 °C) is mostly injected into the overlying NTR (~<2 km in Figure 4d) where it is heated to ~240 °C, and then it migrates downward into HTR, resulting in two maximums of seismicity within the NTR and HTR, respectively (C. W. Johnson et al., 2016; Stark, 2003). According to the conceptual model of Stark (2003), a higher temperature contrast between the injected water and rock in the NTR induces much

stronger thermoelastic effects than in the HTR. Strong thermoelastic effects can promote opening of small thermal cracks adjacent to the main fracture and form a joint fracture system (Ghassemi, 2012; Perkins & Gonzalez, 1985). The presence of these small thermal cracks enhances the frequency dependence of tensile rupture in the source as discussed in the previous section (Figure 4e). This explains the distinct distribution of events with an extra significant increase of ISO with f_u and its correlation with the injection points in depth. For an enhanced geothermal system, thermoelastic effects induced by the cool water injection dominate around the injection well and the liquid water zone created by the injection, whereas the poroelastic effects are more important for inducing the microseismicity at distance from the injection wells (Jeanne et al., 2014; Kwiatek et al., 2015; Martínez-Garzón et al., 2014; Rutqvist et al., 2016). The events with a weak frequency dependence of the ISO may be less influenced by thermoelastic effects but more by poroelastic effects.

4. Discussion and Conclusions

Our analysis of induced microearthquakes in The Geysers region reveals that the retrieved MTs depend on the frequency band of the inverted waveforms. The observed frequency dependence of MTs can provide insight into the details of source processes and involvement of fluids during fracturing. The significance of the frequency dependence is quantified for different properties calculated using the MTs. While the fault plane solutions are rather frequency independent, the percentages of the DC, CLVD, and ISO components change significantly with the frequency band of inverted waves. Frequency dependence should be taken into account when studying the physical processes related to different components of MTs.

The average RMS of MTs obtained in different frequency bands shows a close correlation with the spectra of the ambient noise and the S/N ratio, which implies a strong impact of noise level on the misfit of the MT inversion. Such data misfits caused by nonphysical factors can be prevented by the PCA-based approach from being passed to the retrieved MTs. Statistical variations of MTs depict the frequency-dependent source process.

The percentages of the DC and ISO components tend to decrease and increase with the upper cutoff frequency, respectively. This implies that shear rupture radiates energy preferentially in a lower frequency band and tensile rupture in a higher frequency band. This is consistent with previous studies on the source mechanisms of induced earthquakes and suggests that shear and tensile ruptures preferentially occur on different spatial scales. Such observations support the interpretation of a source model with a main shear fracture and smaller tensile cracks adjacent to the main fracture.

Thermoelastic and poroelastic effects caused by the fluid injection and migration control the occurrence of induced seismicity on different spatial and temporal scales. This is indicated by the frequency dependence of the ISO component. A significant portion of events display a strong increase of the ISO with the upper cutoff frequency. These events are mostly confined within the same depth interval as the injection points, where much stronger thermoelastic effects are expected than in the deeper reservoir due to a higher temperature contrast between the injected water and rock. Hence, the frequency dependence of the ISO component might be produced by small thermal cracks induced by thermoelastic effects in rock close to injection points.

References

Beall, J., & Wright, M. (2010). Southern extent of The Geysers high temperature reservoir based on seismic and geochemical evidence. *Geothermal Resources Council Transactions*, *34*, 1199–1202.

Beall, J., Wright, M., Pingol, A., & Atkinson, P. (2010). Effect of high rate injection on seismicity in The Geysers. *Geothermal Resources Council Transactions*, *34*, 1203–1208.

Boyd, O. S., Dreger, D. S., Gritto, R., & Garcia, J. (2018). Analysis of seismic moment tensors and in situ stress during Enhanced Geothermal System development at The Geysers geothermal field, California. *Geophysical Journal International*, *215*(2), 1483–1500. https://doi.org/10.1093/gji/ggy326

Boyd, O. S., Dreger, D. S., Lai, V. H., & Gritto, R. (2015). A systematic analysis of seismic moment tensor at The Geysers Geothermal Field, California. *Bulletin of the Seismological Society of America*, *105*(6), 2969–2986. https://doi.org/10.1785/0120140285

Dellinger, M., Majer, E. L., Freeman, K., Johnson, L., Jarpe, S., Nihei, K., et al. (2017). Monitoring the effect of injection of fluids from the Lake County Pipeline on seismicity at The Geysers, California, Geothermal Field (Report No. FG-36-03GO13048): U.S. Department of Energy. https://doi.org/10.2172/1410331

Ghassemi, A. (2012). A review of some rock mechanics issues in geothermal reservoir development. *Geotechnical and Geological Engineering*, *30*(3), 647–664. https://doi.org/10.1007/s10706-012-9508-3

Guilhem, A., Hutchings, L., Dreger, D. S., & Johnson, L. R. (2014). Moment tensor inversions of M ~ 3 earthquakes in the Geysers geothermal fields, California. *Journal of Geophysical Research: Solid Earth*, *119*, 2121–2137. https://doi.org/10.1002/2013JB010271

Jeanne, P., Rutqvist, J., Hartline, C., Garcia, J., Dobson, P. F., & Walters, M. (2014). Reservoir structure and properties from geomechanical modeling and microseismicity analyses associated with an enhanced geothermal system at The Geysers, California. *Geothermics*, *51*, 460–469. https://doi.org/10.1016/j.geothermics.2014.02.003

Johnson, C. W., Totten, E. J., & Burgmann, R. (2016). Depth migration of seasonally induced seismicity at The Geysers geothermal field. *Geophysical Research Letters*, *43*, 6196–6204. https://doi.org/10.1002/2016GL069546

Johnson, L. R. (2014a). A source model for induced earthquakes at the Geysers Geothermal Reservoir. *Pure and Applied Geophysics*, *171*(8), 1625–1640. https://doi.org/10.1007/s00024-014-0798-7

Johnson, L. R. (2014b). Source mechanisms of induced earthquakes at The Geysers Geothermal Reservoir. *Pure and Applied Geophysics*, *171*(8), 1641–1668. https://doi.org/10.1007/s00024-014-0795-x

Kinoshita, S. (1994). Frequency-dependent attenuation of shear waves in the crust of the southern Kanto area, Japan. *Bulletin of the Seismological Society of America*, *84*(5), 1387–1396.

Knopoff, L., & Randall, M. J. (1970). The compensated linear-vector dipole: A possible mechanism for deep earthquakes. *Journal of Geophysical Research*, *75*(26), 4957–4963. https://doi.org/10.1029/JB075i026p04957

Kwiatek, G., Martínez-Garzón, P., Dresen, G., Bohnhoff, M., Sone, H., & Hartline, C. (2015). Effects of long-term fluid injection on induced seismicity parameters and maximum magnitude in northwestern part of The Geysers geothermal field. *Journal of Geophysical Research: Solid Earth*, *120*, 7085–7101. https://doi.org/10.1002/2015JB012362

Madariaga, R. (1976). Dynamics of an expanding circular fault. *Bulletin of the Seismological Society of America*, *66*(3), 639–666.

Majer, E. L., & Peterson, J. E. (2007). The impact of injection on seismicity at The Geysers, California Geothermal Field. *International Journal of Rock Mechanics and Mining Sciences*, *44*(8), 1079–1090. https://doi.org/10.1016/j.ijrmms.2007.07.023

Martínez-Garzón, P., Kwiatek, G., Bohnhoff, M., & Dresen, G. (2017). Volumetric components in the earthquake source related to fluid injection and stress state. *Geophysical Research Letters*, *44*, 800–809. https://doi.org/10.1002/2016GL071963

Martínez-Garzón, P., Kwiatek, G., Sone, H., Bohnhoff, M., Dresen, G., & Hartline, C. (2014). Spatiotemporal changes, faulting regimes, and source parameters of induced seismicity: A case study from The Geysers geothermal field. *Journal of Geophysical Research: Solid Earth*, *119*, 8378–8396. https://doi.org/10.1002/2014JB011385

Ohminato, T., Chouvet, B. A., Dawson, P., & Kedar, S. (1998). Waveform inversion of very long period signals associated with magmatic injection beneath Kilauea Volcano, Hawaii. *Journal of Geophysical Research*, *103*(B10), 23,839–23,862. https://doi.org/10.1029/98JB01122

Perkins, T., & Gonzalez, J. (1985). The effect of thermoelastic stresses on injection well fracturing. *Society of Petroleum Engineers Journal*, *25*(01), 78–88. https://doi.org/10.2118/11332-PA

Peterson, J. (1993). Observations and modeling of seismic background noise (Open-File Report 93-322): USGS, US. https://doi.org/10.3133/ofr93322

Ruff, L. J., & Tichelaar, B. W. (1990). Moment tensor rate functions for the 1989 Loma Prieta Earthquake. *Geophysical Research Letters*, *17*(8), 1187–1190. https://doi.org/10.1029/GL017i008p01187

Rutqvist, J., Jeanne, P., Dobson, P. F., Garcia, J., Hartline, C., Hutchings, L., & Walters, M. (2016). The Northwest Geysers EGS Demonstration Project, California - Part 2: Modeling and interpretation. *Geothermics*, *63*, 120–138. https://doi.org/10.1016/j.geothermics.2015.08.002

Sato, T., & Hirasawa, T. (1973). Body wave spectra from propagating shear cracks. *Journal of Physics of the Earth*, *21*(4), 415–431. https://doi.org/10.4294/jpe1952.21.415

Šílený, J. (1998). Earthquake source parameters and their confidence regions by a genetic algorithm with a 'memory'. *Geophysical Journal International*, *134*(1), 228–242. https://doi.org/10.1046/j.1365-246x.1998.00549.x

Šílený, J., Hill, D. P., Eisner, L., & Cornet, F. H. (2009). Non-double-couple mechanisms of microearthquakes induced by hydraulic fracturing. *Journal of Geophysical Research*, *114*, B08307. https://doi.org/10.1029/2008JB005987

Stark, M. (2003). Seismic evidence for a long-lived enhanced geothermal system (EGS) in the Northern Geysers Reservoir. *Geothermal Resources Council Transactions*, *27*, 727–732.

Stierle, E., Bohnhoff, M., & Vavryčuk, V. (2014). Resolution of non-double-couple components in the seismic moment tensor using regional networks—II: application to aftershocks of the 1999 Mw 7.4 Izmit earthquake. *Geophysical Journal International*, *196*(3), 1878–1888. https://doi.org/10.1093/gji/ggt503

Stierle, E., Vavryčuk, V., Šílený, J., & Bohnhoff, M. (2014). Resolution of non-double-couple components in the seismic moment tensor using regional networks—I: a synthetic case study. *Geophysical Journal International*, *196*(3), 1869–1877. https://doi.org/10.1093/gji/ggt502

Udías, A., Madariaga, R., & Buforn, E. (2014). *Source Mechanisms of Earthquakes: Theory and Practice*. Cambridge: Cambridge University Press. https://doi.org/10.1017/CBO9781139628792

Vavryčuk, V. (2001). Inversion for parameters of tensile earthquakes. *Journal of Geophysical Research*, *106*(B8), 16,339–16,355. https://doi.org/10.1029/2001JB000372

Vavryčuk, V. (2002). Non-double-couple earthquakes of 1997 January in West Bohemia, Czech Republic: Evidence of tensile faulting. *Geophysical Journal International*, *149*(2), 364–373. https://doi.org/10.1046/j.1365-246X.2002.01654.x

Vavryčuk, V. (2005). Focal mechanisms in anisotropic media. *Geophysical Journal International*, *161*(2), 334–346. https://doi.org/10.1111/j.1365-246X.2005.02585.x

Vavryčuk, V. (2011a). Detection of high-frequency tensile vibrations of a fault during shear rupturing: observations from the 2008 West Bohemia swarm. *Geophysical Journal International*, *186*(3), 1404–1414. https://doi.org/10.1111/j.1365-246X.2011.05122.x

Vavryčuk, V. (2011b). Tensile earthquakes: Theory, modeling, and inversion. *Journal of Geophysical Research*, *116*, B12320. https://doi.org/10.1029/2011jb008770

Vavryčuk, V. (2015). Moment tensor decompositions revisited. *Journal of Seismology*, *19*(1), 231–252. https://doi.org/10.1007/s10950-014-9463-y

Vavryčuk, V., Adamová, P., Doubravová, J., & Jakoubková, H. (2017). Moment tensor inversion based on the principal component analysis of waveforms: Method and application to microearthquakes in West Bohemia, Czech Republic. *Seismological Research Letters*, *88*(5), 1303–1315. https://doi.org/10.1785/0220170027

Yoshimoto, K., Sato, H., & Ohtake, M. (1993). Frequency-dependent attenuation of P and S waves in the Kanto area, Japan, based on the coda-normalization method. *Geophysical Journal International*, *114*(1), 165–174. https://doi.org/10.1111/j.1365-246X.1993.tb01476.x

Yu, C., Vavryčuk, V., Adamová, P., & Bohnhoff, M. (2018). Moment tensors of induced microearthquakes in The Geysers Geothermal Reservoir from broadband seismic recordings: Implications for faulting regime, stress tensor, and fluid pressure. *Journal of Geophysical Research: Solid Earth*, *123*, 8748–8766. https://doi.org/10.1029/2018JB016251

Zhao, P., Kuehn, D., Oye, V., & Cesca, S. (2014). Evidence for tensile faulting deduced from full waveform moment tensor inversion during the stimulation of the Basel enhanced geothermal system. *Geothermics*, *52*, 74–83. https://doi.org/10.1016/j.geothermics.2014.01.003